



Geochemical fractionation and spectroscopic fingerprinting for evaluation of the environmental transformation of potentially toxic metal(oid)s in surface–subsurface soils

Samina Irshad · Guijian Liu · Balal Yousaf · Muhammad Ubaid Ali ·
Rafay Ahmed · Abdul Rehman · Muhammad Saqib Rashid · Yusra Mahfooz

Received: 26 October 2020 / Accepted: 3 April 2021 / Published online: 15 April 2021
© The Author(s), under exclusive licence to Springer Nature B.V. 2021

Abstract The contamination of soil by toxic metal(oid)s has emerged as a major concern worldwide, particularly in developing countries. A metals behavior in the soil environment is influenced by organic matter, mineral phases, and oxidation states in which a particular metal exists. However, the spectroscopic evidence of metal(oid)s interactions in soil with organic matter and mineral phases can induce an extensive understanding. The surface and sub-surface soils (0–50 cm) from four sites of upper Indus basin,

Pakistan, were collected and analyzed by using FTIR (Fourier-transform infrared spectroscopy), XRD (X-ray diffraction) and XPS (X-ray photoelectron spectroscopy) in addition to ICP-MS (inductively coupled plasma mass spectrometry) and geochemical fractionation. Geochemical fractionation of metal(oid)s indicated that As, Cu, Ni, Pb, and Zn were mostly found in the potentially bioavailable fractions. However, an increase in the residual fraction was observed from top to bottom. The absorption bands of FTIR spectra were divided into three spectral regions 700–400, 1700–800, and 3700–2800 cm^{-1} . The soil was found rich in organic matter and capable of retaining metals

Supplementary Information The online version contains supplementary material available at <https://doi.org/10.1007/s10653-021-00932-z>.

S. Irshad · G. Liu (✉) · B. Yousaf ·
M. U. Ali · R. Ahmed · A. Rehman · M. S. Rashid
CAS-Key Laboratory of Crust-Mantle Materials and
Environment, School of Earth and Space Sciences,
University of Science and Technology of China,
Hefei 230026, People's Republic of China
e-mail: lgj@ustc.edu.cn

S. Irshad
e-mail: saminakhan@mail.ustc.edu.cn

B. Yousaf
e-mail: balal@ustc.edu.cn

M. U. Ali
e-mail: ubaid@mail.ustc.edu.cn

R. Ahmed
e-mail: malikrafay@mail.ustc.edu.cn

A. Rehman
e-mail: abdulrehman008@mail.ustc.edu.cn

M. S. Rashid
e-mail: saqibssr@mail.ustc.edu.cn

S. Irshad · G. Liu
State Key Laboratory of Loess and Quaternary Geology,
Institute of Earth Environment, The Chinese Academy of
Sciences, Xi'an 710075, Shaanxi, People's Republic of
China

Y. Mahfooz
Sustainable Development Study Centre, Government
College University, Lahore, Pakistan
e-mail: sdsc8888@gmail.com

as abundant peaks were observed in the mid-infrared region. The mineralogical analysis of soil samples testified silicon oxides and zeolite as major mineral phases. The XPS spectra showed broad peaks of As(III), As₂O₃, As₄S₄, PbO₂, and PbCO₃. The study concludes that the source identification of metal(oid)s in the upper Indus is crucial to find out the particular source of contamination in the soil.

Keywords Soil · Potentially toxic metal(oid)s · Vertical distribution · Geochemical fractionation · Spectroscopic fingerprinting · Mineralogy

Introduction

The human-induced activities are generally considered as a major source of potentially toxic metal(oid)s (PTMs) contamination in the soil system, leading to the gradual accumulation and resulting in the toxicity of the environment. Consequently, concentrations beyond the adsorption capacity of the soil or the interactions of PTMs with soil surfaces result in the increased toxicity (Zhang et al., 2018). The anthropogenic activities that lead to the outbreak of the concentration of a metal in the environment differ for different metals. The major sources of Pb contamination in the environment are industries and vehicles (Sun et al., 2018). The As contamination in the surface soils may arise from the geogenic sources but man-made activities such as milling, pesticide usage, and gold mining are considered as the main contributors (Rahman et al., 2017). The application of organic and mineral fertilizers to the soil outbreaks in the toxicity of Cd (Van Poucke et al., 2018).

All the metals investigated for total concentration and distribution in the soil profile have varied pathways in the environment, dependent upon many factors (Rehman et al., 2020). The total concentration of a metal in any environment could not give information regarding the physical and chemical behavior of metal. The presence of a metal in the soil environment in mobile or potentially mobile fractions signifies the severity of contamination. Therefore, it is essential to investigate the bioavailable fractions of metal(oid)s in the soil (Gmochowska et al., 2019).

Soil is a complex environment which contains both primary and secondary minerals. Primary minerals

originate from the soil parent material, and the occurrence of clay minerals is regulated by the process of weathering (Butler et al., 2018). The mineral phases present in a soil environment are directly or indirectly associated with physical, chemical, and biological properties. In recent years, spectroscopic investigations have emerged as time saving and effective techniques to study soil properties. The spectroscopic techniques are non-destructive, require minimum sample preparation, and are capable of delivering the most reliable results (Xing et al., 2016). FTIR is a prospective technique for qualitative and quantitative estimation of the organic and inorganic functional groups present in the soil. The soil functional groups have a vital function in metal-binding (Dhillon et al., 2017). The functional groups in the soil such as polysaccharides, aromatics, and amides are considered as the most sensitive groups for metal binding (Wen et al., 2018). XRD (X-ray powder diffraction) is a non-destructive and rapid technique to quantitatively analyze the mineral composition of the soil. The chemical speciation of metals is considered as an effective tool for the analysis of a metal's behavior in the soil system (Wan et al., 2016). The chemical state of a particular metal is strongly associated with its transportation and mobility in a soil environment. The bioavailability of metals is strongly associated with the state of occurrence in soil. X-ray photoelectron spectroscopy (XPS) is the most extensively used technique for chemical speciation analysis of metals (Lilli et al., 2019).

The rapid urbanization and industrialization resulted in soil and water contamination in the Indus valley. However, many studies have been conducted in the lower Indus region of Pakistan asserting soil and water contamination (Farooqi et al., 2007, 2009; Shahid et al., 2018). The developmental activities in the upper Indus region such as extensive agricultural practices, urbanization and industrialization may have significantly altered the soil physicochemical properties, particularly extensive mining and agricultural practices in the vicinity of Abbottabad, agricultural and Industrial activities in Haripur and Attock, urbanization and industrialization in Islamabad. However, little knowledge is available regarding the contamination status of the soil. Therefore, a comprehensive analysis of upper Indus region was carried out by analyzing soils for concentration of As, Cd, Cr, Cu, Fe, Mn, Ni, Pb, Sr and Zn, geochemical fractionation

and spectroscopic techniques. The selection of metal(oid)s was based on their hazardous nature, perseverance, bioaccumulation and residence time in soil. The present study aimed to (1) characterize the soil profile of 0–50 cm depth for the PTMs concentration and investigation of contamination status in the surface soils, (2) to investigate the interfacial behavior of metal(oid)s in soil profile through geochemical fractionation, and (3) to carry out the spectroscopic fingerprinting of soil profile by FTIR, XRD, and XPS.

Materials and methods

Site description and sample collection

The soil samples were collected from four cities of upper Indus valley (northern region), Pakistan, i.e., Abbottabad (A), Haripur (B), Attock (C), and Islamabad (D) (Fig. S1). The soil texture of site A is classified as sandy loam and silt loam (Jadoon et al., 2020), site B as silt clay loam (Tariq et al., 2011), site C as sandy loam and loam (Obaid-ur-Rehman, 2010), and site D as silty loam (Ali & Malik, 2010). The study area is about 11,457 km² and the population is about 44.25 million (Husnain, 2016). The climatic conditions of the study area are arid to semi-arid. The annual flow of the upper Indus River is around 4 million m³. Pakistan being an agricultural country with an annual production rate around 90% is solely reliant on irrigation, and 70% of the irrigation water is provided by Indus basin irrigation network (IBIN). However, agricultural activities as well as rapid urbanization and industrialization in the upper Indus valley have ultimately affected the water and soil quality (Irshad et al., 2019). Therefore, this study is designed to study the metals behavior, pollution status, and mineralogy in a 0–50 cm soil profile. The samples at site A and B were collected from agricultural soils, site C from urban and site D from an industrial area.

A total of 550 samples were collected from 110 sites of the study area at different depths (0–10, 10–20, 20–30, 30–40, 40–50 cm) during January–March 2017. The 50 g of soil were collected at every sampling point by using a soil sampler and applying the zigzag sampling technique (Parab et al., 2015). For one sampling point, 4 samples were collected at a distance of 1 m and a composite bulk sample was prepared. Subsequently, 3 subsamples were prepared

for each sampling point. To calculate the background values, samples were collected from undisturbed sites of each location with least human interventions (Table S1) and provided in our previous study (Irshad et al., 2019). The soil samples were air-dried, homogenized, and properly sieved (< 2 mm) before geochemical fractionation. The soil samples (one-fourth of each sample) were oven-dried at 105 °C for 24 h, grounded using a ceramic soil-pulverizer mill machine, and sieved through 200 mesh. The samples were stored in airtight bags and kept under freezing temperatures before further analysis.

Sample preparation and characterization

The EC and pH of soil samples were measured by preparing soil saturated extract through digital EC and pH meter (EC 300, pH 100, YSI Company). For the estimation of the total concentration of PTMs at four sites, 0.2 g of sample was taken in the digestion flask and digested by adding aqua regia (Rehman et al., 2018). After preparation, the samples were tested using high-precision Agilent 7500cx ICP-Mass Spectrometer for the total concentration of PTMs. The targeted PTMs As, Cd, Cr, Cu, Fe, Mn, Ni, Pb, Sr, and Zn were tested using ICP-MS (Agilent 7500cx). To calibrate the instrument, a stock solution for multiple elements, 1, 2, 4, 6, and 10 mg/L was prepared. To find out the elemental input by reagents used in the sample preparation process, initially two blank samples with no contamination were analyzed. To estimate the accuracy of the instrument, multiple-element working solutions were analyzed.

Geochemical fractionation of PTMs

The soil samples collected from four different locations were sequentially extracted by employing a modified eight-step procedure to determine the geochemical fractions of PTMs (El-naggar et al., 2018). The edition of sulfide fraction was based on suggestions by (Ma & Rao, 1997). To obtain the soluble and exchangeable fractions and taking into consideration the alkalinity of the soil, 1 M NH₄NO₃ (pH 4.8) was substituted by 1 M NH₄-acetate (pH 7.0). Firstly, 50 ml of extractant was added to 2 g of soil, and the mixture was placed on an end-over-end rotator at 20 rpm. After each successive extraction, samples were centrifuged for 10 min at 5000 U/min and were

filtered with 0.45- μm membrane filters. The specific procedure adopted for modified eight-step sequential extraction is described in Table S3.

Enrichment factor (EF)

EF (Eq. 1) is calculated for the investigation of pollution status and to distinguish the pollution source if it is geogenic or anthropogenic (Thiombane et al., 2019). EF was calculated for 0–10 cm soil samples.

$$EF = \frac{[X/Fe]_{\text{Sample}}}{[X/Fe]_{\text{Background}}} \quad (1)$$

Commonly used PTMs for geochemical normalization include manganese, titanium, aluminum, and iron. However, Fe was used as geochemical normalization factor in the present study due to having similar geochemistry with most of the PTM's, naturally uniform occurrence and also for the reason that it is found in combination with other trace elements (Rehman et al., 2018; Wang et al., 2015).

Geo-accumulation index (I_{geo})

The I_{geo} index can be applied to investigate the accumulation of a particular element at a specific site (Müller, 1979; Shaheen et al., 2019). The I_{geo} model categorizes PTMs pollution into seven enrichment classes. Based on this model, metal(oid)s are described as un-contaminated to extremely contaminated (Sun & Chen, 2018). I_{geo} of targeted metals in 0–10 cm soil was assessed by using Eq. 2:

$$I_{\text{geo}} = \log_2 \left[\frac{C_n}{1.5 \times B_n} \right] \quad (2)$$

In the above equation, C_n shows the elemental contents in the presented sample, and B_n refers to the background value of that specific element.

FTIR spectroscopy

The MIR spectra of sieved soil samples from 4 sites at 5 different depths were collected over a range of 400–4000 cm^{-1} at a resolution of 4 cm^{-1} by using a Nicolet 8700 Fourier transform infrared spectrometer. Around 2 mg of soil sample was weighed and ground with 100 mg of KBr into powder form and mixed. After that, the prepared mixture was pressed and a

pellet of diameter 1 cm was made by a hydraulic tablet machine. A total of 16 scans for a sample were taken to reduce the chance of error in the spectra. Data obtained from FTIR spectra were processed by using OMNIC software Nicolet (6.1a), and spectral deconvolution for the estimation of peak positions in the full spectra and desired wavelength (1700–700 cm^{-1}) was done by using the professional version of Peakfit v4.12.

Soil mineralogy

The mineralogical analysis of soil from four sites was executed by powder X-ray diffraction (XRD). Samples from all three sites were scanned by Philips X Pert Pro (Cu $K - \alpha$) XRD on a fraction of size < 2 μm with a targeted voltage of 40 kV. The emission current produced was about 30 mA along the scanning angle of 10°–70° over 20 intervals at a rate of 0.1°. The XRD analysis was done by using Xpert HighScore plus by putting the limitation as mineralogy to study the mineral phases of soil.

XPS

The surface chemistry and bonding states of PTMs in soil samples at five different depths have been calculated using ESCLAB 250xi, Thermo Fisher Scientific. The chemical composition and state of soil at an area of 0.5 \times 0.5 mm^2 , the monochromated Al $K \alpha$ X-ray (1486.68 eV) source were used at 150 kV and 20 mA. The spectra produced was observed around 1100 eV at a resolution of 1 eV, whereas the narrow-high resolution scans of Fe 2P, As 3d and Pb 4f were recorded at pass energy of 30 eV. The spectra obtained by XPS were fitted using the windows version of XPSPeak41.

Quality assurance and data precision

The quality control for extraction of metalloids was executed by using certified soil reference materials (CRM051 and CRM042) under the recovery rate of 86–95%. To achieve the accuracy of sequential extraction, sum of eight fractions was compared to results obtained from total metal concentration. Recovery = 100 $(F1 + F2 + F3 + F4 + F5 + F6 + F7 + F8)/\text{total concentration}$. To ensure the reliability of results of blank, triplicate measurements were taken in the

analysis. For quality assurance of the total concentration, the National Center for standard material of China’s reference material (GBW07406) was used in this study. Standard reference material with a recovery rate of 96.4–102.3% was found to be in the certified limits of all the elements studied. To ensure the accuracy of the method adopted, the recovery range optimized was around 92.12–102.7% with a precision level of ± 5 wt% and linear calibration curves in the range of ($R^2 < 0.99$). For graphical presentation of the data, SigmaPlot 11.0 and origin 2018 were used.

Results and discussions

Vertical distribution of PTMs in soil

The vertical distribution pattern of PTMs at depths 0–50 cm is depicted in Fig. 1. Each element showed a different distribution trend, although on average the metals exhibited a downward migration trend. Generally, the metal concentration increased initially and

decreased with the depth of the soil. However, the vertical distribution trend of a particular metal varied from site to site. The fluctuations of PTMs concentration at different sites may be credited to either the natural variability or inputs from anthropogenic sources. The vertical migration trend of PTMs is significantly affected by the chemical and physical structure of soil (Li et al., 2019). The pH of the soil samples ranged from 6.12 to 8.86. (Table S2).

The depth profile of As varies significantly among four sites. The concentration of As increased initially in case of site C at 10–20 cm and at 30–40 cm for A and B, after that concentration of the metal decreased significantly toward the bottom. The elevated levels of As in the soil of study area may occur as a result of industrial wastes and agrochemical usage (Shahid et al., 2018). The concentration of Cr in four sites also decreased from top to bottom but at C increased at 20–30 cm significantly and then decreased toward the bottom. In general, the concentration of most of the elements increased at a depth of 20–40 cm and decreased subsequently. Most of the PTMs were

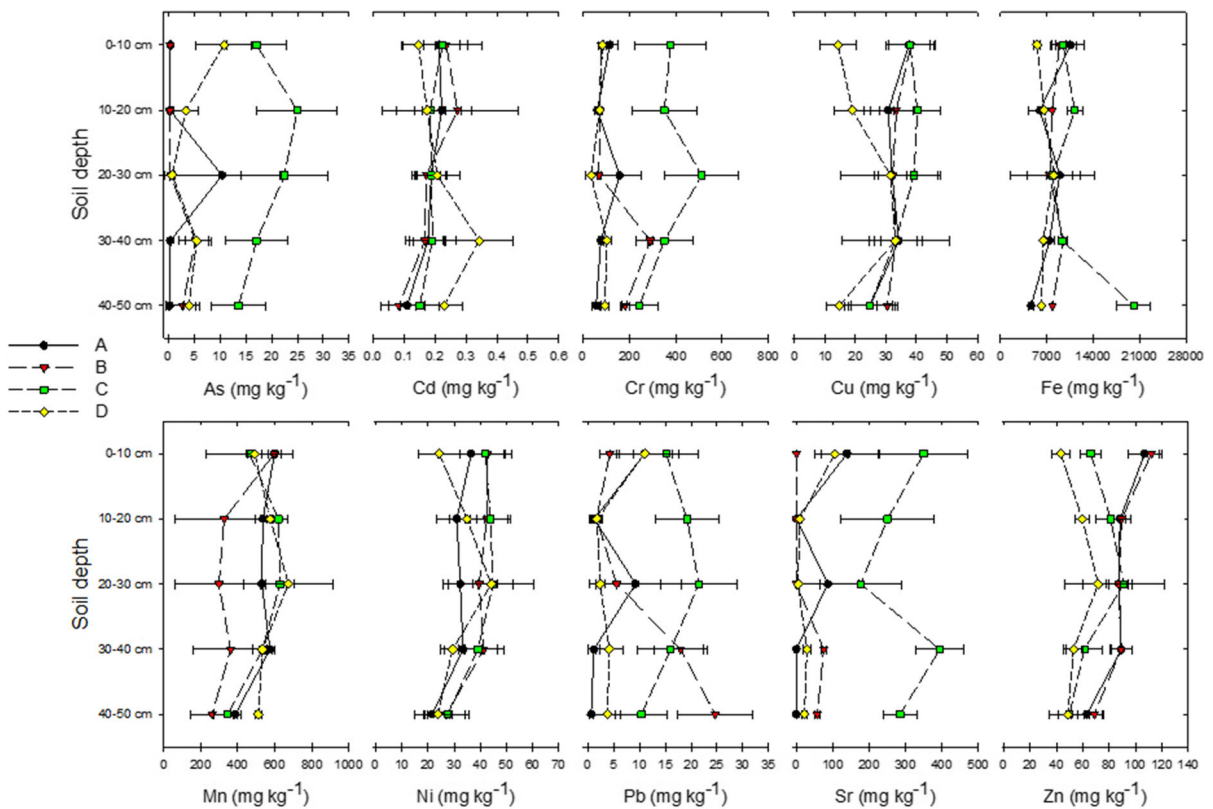


Fig. 1 Vertical distribution of PTMs in soil from **a** Abbottabad, **b** Haripur, **c** Attock and **d** Islamabad

found deeply enriched in the 0–40 cm layer. However, maximum values appeared in 10–30 cm depth (Zhou et al., 2014). In the current study the maximum value of As at site A was observed at 20–30 cm, B at 30–40 cm, C 10–20 cm, and D at 0–10 cm. It has been observed that the concentration of various PTMs such as As, Cd, Hg, Pb, and Zn declined beyond the depth of 25 cm in non-emended soil samples (Bidar et al., 2016).

PTMs are mostly bounded in clay layers and fine particles of soil, hence are usually found with higher concentrations in the upper layer credited to anthropogenic activities (Zhou et al., 2014). Generally, all of the elements were found accumulated in the 0–40 cm layer (Zhou et al., 2014). Current study results are in line with these results as with different distribution patterns, all the elements were found accumulated from 0–40 cm and declined subsequently. The concentration of elements in a vertical profile of 0–50 cm was not stable. This could be attributed to the fact that a stable concentration of PTMs could be found below 60 cm depth, indicating that the chemical structure of deeper layers reflects the geochemical background of drainage sink (Zhou et al., 2014). The capability of PTMs migration is dependent on proportion; Zn, Cr, and Pb showed a strong migration capability as compared to Cu. The migration ability of elements decreased beyond one meter (Zhang et al., 2018). PTMs are strongly capable of absorption onto clay minerals. The sediments and soil having a higher content of clay minerals, result in low redox potential environment. Therefore, the ability to exchange oxygen in such an environment decreases markedly as compared to the coarse sediments and soil particles (Bonetti et al., 2017).

Geochemical fractionation of PTMs in soil

The total metal contents are not considered as reliable indicators of the severity of metal pollution at a particular site. Therefore, an eight-step modified sequential extraction of PTMs for five different depths was carried out (Fig. 2). The metals in soluble and carbonate bound fractions can easily migrate and could be absorbed by plants. Under low pH, the metals in these fractions can easily discharge into the environment (Sun et al., 2018). However, in the current study, *F1* was not the dominant fraction for most of the metal profiles. Nevertheless, Mn showed a

significant percentage of metal fractions bound to soluble and exchangeable, i.e., 5–12%, 4–14%, 3–9%, and 5–8% at sites A, B, C, and D, respectively. Sr also showed a significant percentage in *F1* but only at the top layer and comprised of 20% at site A, 1.4% at site B, 9% at site C and 12% at site D. Cu and Zn showed a significant percentage of metals bound to carbonate fraction throughout the soil profile at all sites. The mobile forms of Pb and Ni mostly dominated in Mn and Fe oxide fractions at all sites. However, the residual Pb and Ni generally dominated in 30–50 cm depths. Previously the mobile forms of Pb were found bound to the reducible fraction. (Gmochowska et al., 2019). The metals retaining with Fe and Mn oxides could be a source of long-term contamination when a change in oxidation states of Fe and Mn occurs. It is also dependent upon the biological effectiveness of Fe–Mn oxides (Sun et al., 2018). However, the alkaline nature of the soils in these areas could reduce the toxicity of metals, Pb could be more toxic when the soil solution turns to acidic. Distributions of As fractionation at four different sites revealed that at site A the dominant As fractionations (47–89%) were found in residual fractions for all five depths. Mobile forms of As were mostly found at site B, C and D. As was mostly found bound to amorphous and crystalline Fe oxide fractions at site B and D. Many studies have revealed that the Al, Fe and Mn oxides and hydroxides are important scavengers of As in the environmental samples (Wan et al., 2017). The high concentration of As in these fractions could be due to the high concentration of Fe. However, at site C significant percentage of As was found in the organic matter (12–15%) and sulfide (7–26%) fractions, followed by the residual fraction (38–58%) in the soil profile. This shows that As at site C is mostly related to organic matter and sulfide fractions. Organic matter and sulfide fractions play a key role in the mobility and bioavailability of metals (Sun et al., 2018). Cr and Ni showed the metal contents bound to sulfide fractions throughout the soil profile but generally sulfide fraction was not the dominant fraction for most of the metals. However, organic matter was one of the dominant fractions for As at site C, Cd at site B, C, D, and for Cu, Ni and Zn at all sites throughout the soil profile. Elements retaining in organic matter fraction, bind itself to different forms of organic matter by complexation (Sun et al., 2018).

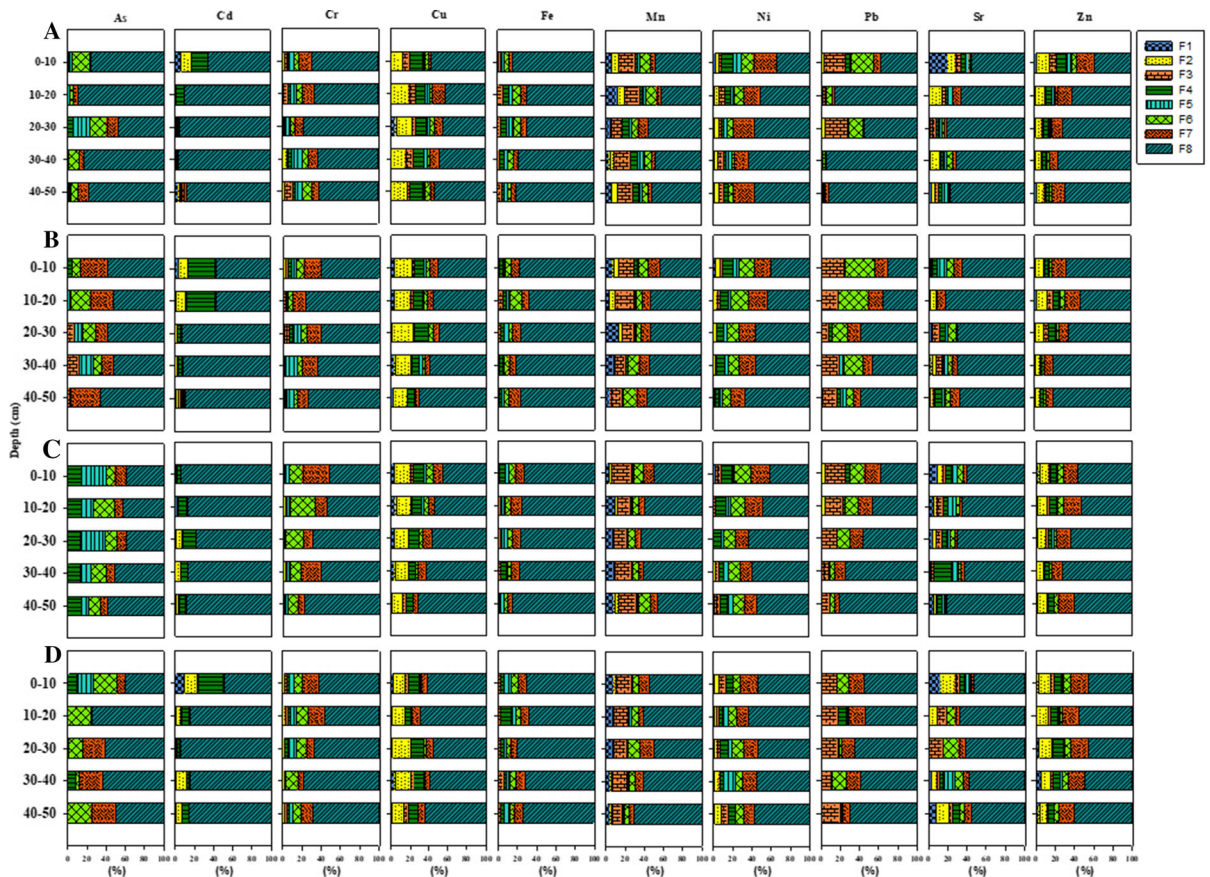


Fig. 2 Geochemical fractionation of PTMs in soil profile. **a** Abbottabad, **b** Haripur, **c** Attock and **d** Islamabad. F1: soluble + exchangeable; F2: carbonate bound; F3: manganese

oxide fraction; F4: sulfide fraction; F5: organic matter; F6: amorphous Fe oxide fraction; F7: crystalline Fe oxide fraction; F8: residual fraction

Pollution indices

Enrichment factor (EF)

The broader picture of EF calculated of the soil samples from four sites at 0–10 cm depth is depicted in Fig S2. EF could serve as a preliminary indicator of PTMs contamination source (Ruiz-Fernández et al., 2019). EF values ranging from 0.5–1.5 predict that metal pollution is solely due to lithogenic or geogenic processes, while EF exceeding 1.5 indicates the human interventions involved in the high concentration of metal (Thiombane et al., 2019). EF values ranging from 1–2 also suggest that the enrichment of metal could be subjected to variations in the pedo-geochemical characteristics of soil, whereas EF > 2 strongly favors the accumulation of metal by anthropogenic sources (Ruiz-Fernández et al., 2019). The EF

values for most of the elements at site A were in the range of 1.03–1.42 suggesting geogenic procedures involved except Ni (2.45), Cd (1.94), and Pb (10.55) indicating anthropogenic activities involved in the metal enrichment. The Cd and Ni intoxication at site A could be attributed to weathering/erosion/leaching of phosphate ore and mining and agricultural activities, respectively. The phosphate ore in the vicinity of site C is reportedly having higher concentrations of Cd in the form of gangue (Jadoon et al., 2020). At site B, EF values for other elements ranged from 0.2 to 1.4 except As (2.18) and Pb (3.56). EF values for C site were in the range of 0.6–1.2 except Cr (3.52), Sr (4.37), Pb (4.13), and As (6.64) being highly enriched due to anthropogenic sources. At site D, EF values ranged from 1.02–1.4 except Mn (1.81), Cd (1.94), Sr (6.65), As (6.67), and Pb (8.33) as highly enriched. The contamination source of As in B, C and D could be

unidentified anthropogenic activities, presenting alarmingly high enrichment of metal in the soil. Moreover, Pb is a highly enriched metal in all study areas. Similarly, in Karachi, Pakistan, the soils were found enriched with Pb (Karim et al., 2015). Previously, Zn, Mn, Li, Ca, Co, Cd, and Pb have been found significantly enriched in the soils of site D due to anthropogenic sources (Iqbal & Shah, 2011).

Geo-accumulation index (I_{geo})

The contamination status of targeted metals has also been assessed by applying the geo-accumulation index, depicted in Fig. 3. The I_{geo} of site A was less than 1 stating un-contamination excluding Ni (1.23) and Pb (3.14), which indicate moderate contamination

and heavy contamination, respectively. At B, I_{geo} values for PTMs ranged from -2.7 to 0.2 asserting the un-contamination of these elements except Pb (1.47) depicting moderate contamination. In C, all other elements were below 0 except for Cr (1.6), Sr (1.8), Pb (1.8) and As (2.5). The I_{geo} model results of C revealed that there is moderate contamination of Cr, Sr, and Pb, whereas As is classified as moderate to heavily contaminated. The I_{geo} values for all other PTMs ranged from 0.09 – 0.94 categorizing un-contamination to moderate contamination, whereas the I_{geo} values for As, Sr, and Pb were 2.65 , 2.63 , and 2.94 , respectively. As and Sr contamination testified in D is moderate, while Pb is considered as moderately to heavily contaminated. Previously Sr was categorized as uncontaminated and Pb as moderately

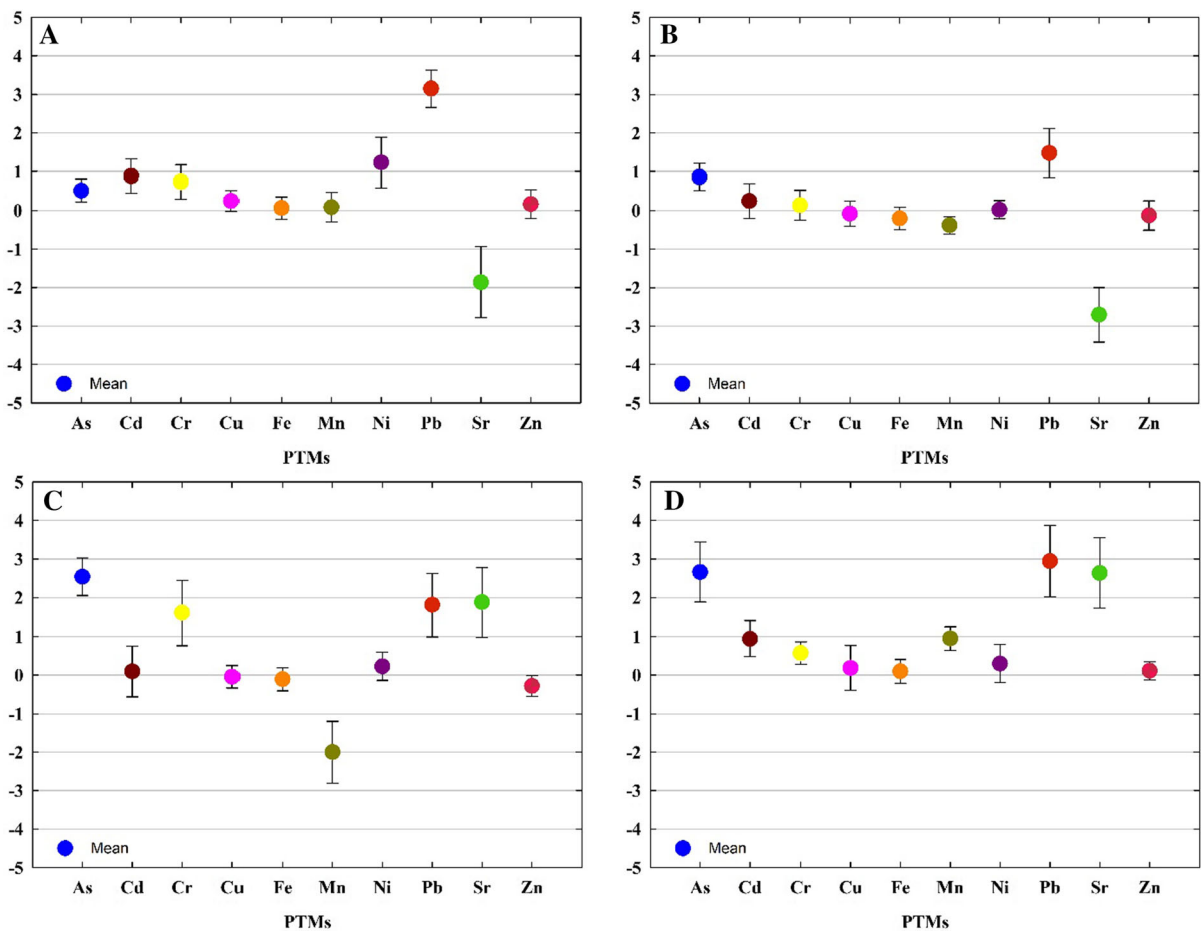


Fig. 3 Geo-accumulation index of PTMs in four cities **a** Abbottabad, **b** Haripur, **c** Attock, **d** Islamabad ($I_{geo} \leq 0$ (no contamination), $0 < I_{geo} < 1$ (uncontaminated to moderately contaminated), $1 < I_{geo} < 2$ (moderately contaminated), $2 < I_{geo}$

< 3 (moderately to heavily contaminated), $3 < I_{geo} < 4$ (heavily contaminated), $4 < I_{geo} < 5$ (heavily to extremely contaminated), $5 < I_{geo}$ (extremely contaminated))

contaminated in soils of site D (Iqbal & Shah, 2011), but in the current study, the contamination status of both metals has significantly changed and it is also noteworthy that the soil at all sites is contaminated with Pb. Karachi is the most urbanized city of Pakistan and has been categorized as moderately contaminated with Pb (Karim et al., 2015).

FTIR analysis

The FTIR spectra of soil samples at five different depths were calculated for a spectral range of 4000–400 cm^{-1} (Fig. 4). The visual observation of soil spectra for different depths in all areas is almost the same irrespective of depth, showing overlapping peaks of heterogeneous components such as soil organic matter and minerals. Therefore, the absorption bands of soil spectra were divided into three main spectral regions based on visual observation, i.e., 700–400, 1700–800, and 3700–2800 cm^{-1} , and bands were assigned according to the previous literature (Table 1). The absorption bands between 2800–3700 cm^{-1} were assigned to O–H and N–H stretching vibrations of water and organic materials such as alcohols, phenols, and amides. The main peaks in this region for four sites at different depths were

observed around 3423–3435 cm^{-1} . The region with abundant peaks was around 800–1700 cm^{-1} generally attributed to the chemical structure of soil organic matter. The peaks observed in this region between 1632 and 1631 cm^{-1} were assigned to N–H bending vibrations of amine and aromatic C=C stretching and C=O stretching from carboxylic acids (Xing et al., 2016). The peaks produced around 1429–1420 cm^{-1} appeared due to the existence of carbonates (Chauhan et al., 2018). The C–O stretching vibration of alcohols, ethers, phenols, and carboxylic acids, and C–O stretching of polysaccharides was observed in the region 1300–1000 cm^{-1} . The distinct peaks in this region were observed at 1081–1018 cm^{-1} at 0–50 cm depth in four areas. The organic functional groups such as amides, hydroxyl, carboxyl, and phenols have the highest active sites for complexation of metals (Dhillon et al., 2017). The wavenumbers below 900 cm^{-1} are generally credited to the absorption of minerals such as quartz and iron oxides along with the C–H vibrations in aromatics (Xing et al., 2016). The peaks at 875–876 cm^{-1} were assigned to vibrations of CO_3^{2-} in calcite and minerals of the calcite and dolomite groups. The absorption bands that appeared around 797–712 cm^{-1} are credited to symmetric stretching of Si–O in inorganic materials (quartz and

Fig. 4 FTIR spectra of soil samples from 0–50 cm depth of four cities a Abbottabad, b Haripur, c Attock, b Islamabad

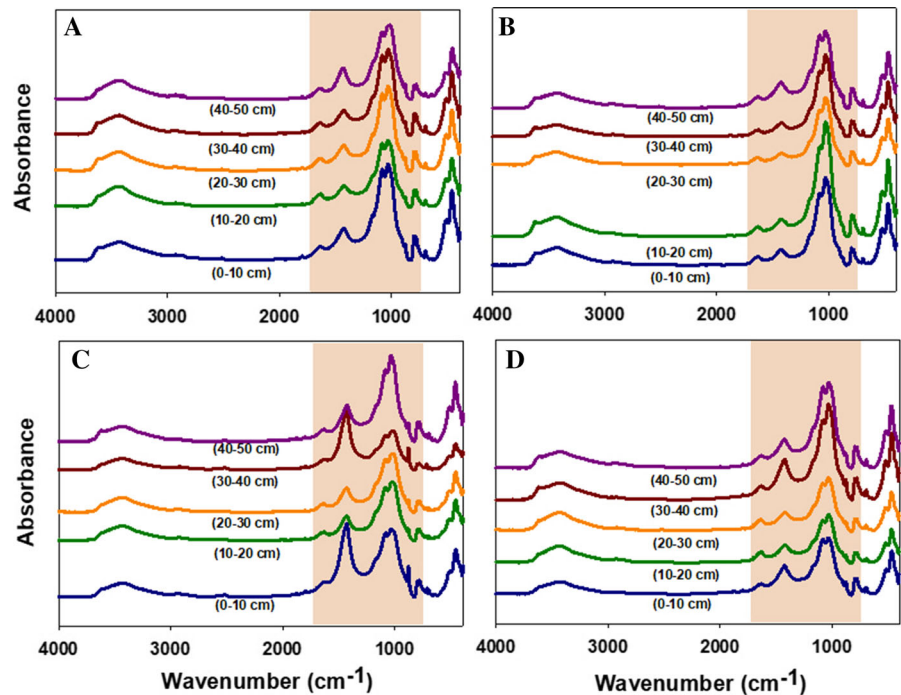


Table 1 Assignment of absorption bands based on previous literature

| Peaks observed | Literature | Bands assigned | References |
|----------------|----------------------------|---|-----------------------|
| 463–471 | 460–470 | Si–O–Si bending in kaolinite, illite, smectite | Chauhan et al. (2018) |
| 516–521 | 520 | Si–O–Al bending | Chauhan et al. (2018) |
| 694 | 675–900 | Out-of-plane bending of the aromatic ring C–H bonds | Bernier et al. (2013) |
| | 690 | Iron oxides | Xing et al. (2019) |
| 712–797 | 715–712 | Fundamental vibrations of CO ₃ ²⁻ in calcite | Bernier et al. (2013) |
| | 783 | Primary amine | Xing et al. (2019) |
| 875–876 | 887–866 | Vibrations of CO ₃ ²⁻ in calcite and minerals of the calcite and dolomite groups | Bernier et al. (2013) |
| 1018–1081 | 1080 | Polysaccharides C–OH | Bernier et al. (2013) |
| | 1300–1000 | In-plane bending of the aromatic ring C–H bonds; the C–O stretching vibration in alcohols, ethers, phenols, carboxylic acids and esters; stretching of C–O in polysaccharides; C–N stretching vibrations in aliphatic and aromatic amines | |
| 1420–1429 | 1420–1425 | Carbonates | Chauhan et al. (2018) |
| 1631–1632 | 1600–1750 cm ⁻¹ | Aromatic C=C stretching, C=O stretching from carboxylic acids, and N–H bending vibrations of amine | Xing et al. (2016) |
| 3423–3435 | 3500–3000 cm ⁻¹ | O–H and N–H stretching vibrations of water and organic materials (alcohols, phenols, and amides) | Xing et al. (2016) |

clay) calcite and carbonates. (Chauhan et al., 2018). The peak attributed to metal oxides and carbonates was observed at 694 cm⁻¹, which appeared at the same wavenumber in all the samples. The Si–O–Al bending vibrations produced the peaks around 521–516 cm⁻¹ and Si–O–Si bending formed the peaks at the wavenumber of 471–463 cm⁻¹. The overall spectral analysis of FTIR bands revealed that the main components of soil were organic matter, clay minerals, and water as the abundant peaks were observed in the mid-infrared region. The soils having a higher amount of organic matter are more capable of retaining metals (Miles & Changwen, 2014).

Soil mineralogy

XRD analysis was performed to study the predominant minerals in a soil profile of 0–50 cm. XRD spectra revealed that soil was mostly composed of crystalline phases. Quartz was the major mineral found in all the soil profiles, but the rest of the mineralogy of soil varied from one site to another (Fig. 5). This could be due to the difference in geographical features of these sites. The main mineral phases present in the surface soils of site A are zeolite and silicon oxides. The main peak of quartz was found at 26.8–26.9 at five depths,

but the height of the peak varied. The intensity of an XRD peak is proportional to the concentration of a particular mineral in the soil (Jozanikohan et al., 2016). Previously, it is reported that quartz was a dominant part of sand and silt fractions (Ferreira et al., 2018). The 10–20 cm soil was rich in quartz but few peaks of bowieite and birnessite were found which were absent in the rest of the soil profile. In the 30–40 cm depth of site A, chalcocopyrite, chalcophanite and montmorillonite were also found. Chalcocopyrite is a common mineral of naturally occurring Cu (Singh & Agrawal, 2012). The montmorillonite and quartz peaks were found in the 40–50 cm depth. In the case of site B, the surface soil showed the maximum peaks of quartz and it is apparent from Fig. 4 that quartz is overlapping other peaks and one peak of ferritapioilite was observed which is absent in rest of the soil profile. The peak position of the main peak of quartz in this area was 26.9–27 with varied height at different depths. The rest of the soil minerals found in this site were zeolite, calcite, niningerite, magnesium calcite, and montmorillonite. The main peak of quartz at site C appeared at 26.9 for all samples. At the site C (0–10 cm) soils, quartz was a major mineral followed by zeolite and calcite and peaks of calcite were seemed to be overlapped by quartz. The rest of the minerals

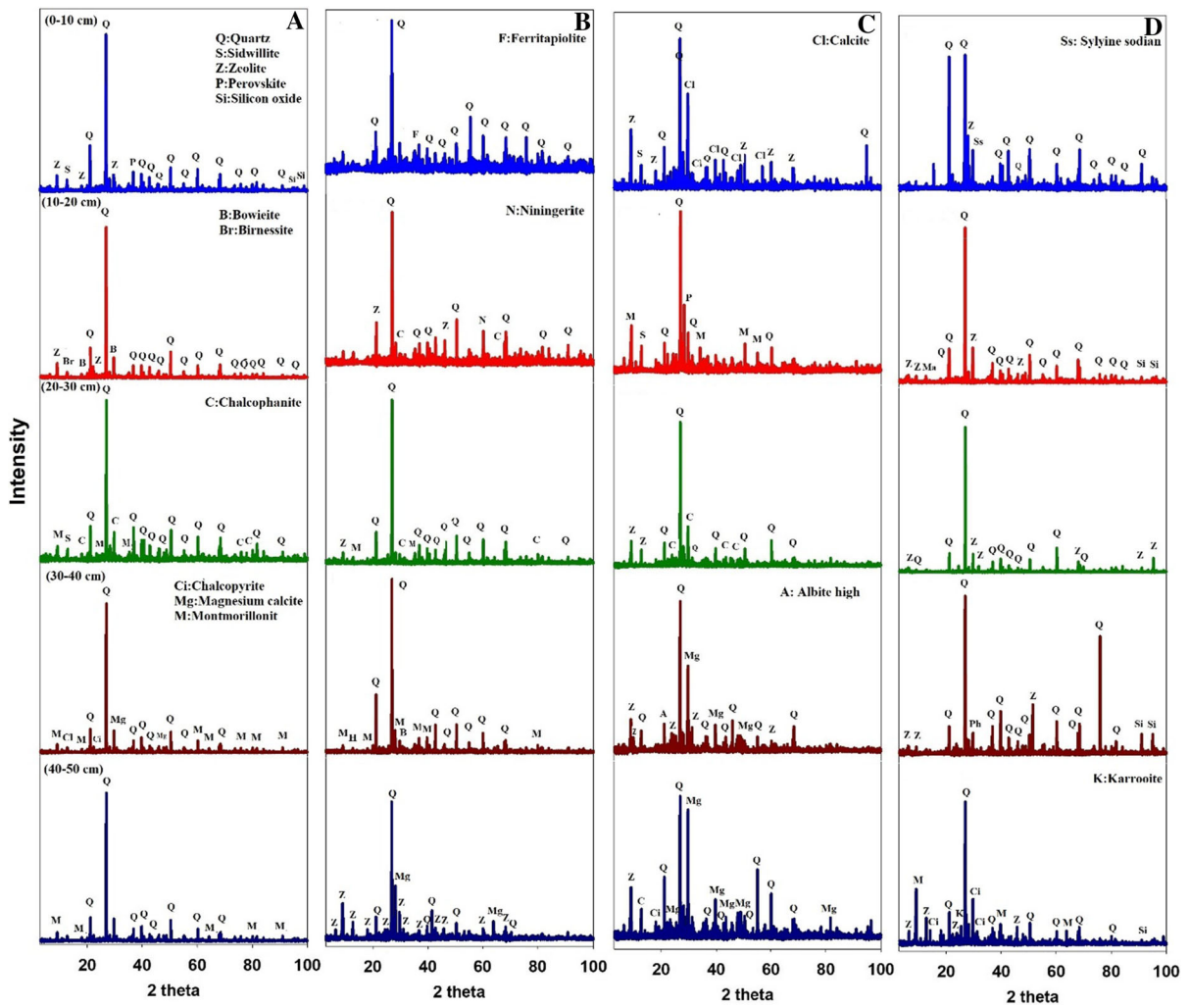


Fig. 5 Soil samples from 0–50 cm depth of four cities **a** Abbottabad, **b** Haripur, **c** Attock, **d** Islamabad

found in this site were perovskite, montmorillonite, sidwillite, and magnesium calcite. At site D, the soil mineralogy was found rich in quartz followed by zeolite, sylvine sodian, karrooite, calcite and montmorillonite. The main peak for quartz in this area for all the samples was found at 26.8–26.9. However, the overall mineralogy of a particular site was same in terms of depth. Quartz was found to be the main mineral at all locations followed by other minerals.

Metal speciation by XPS

The XPS spectra of As_{3d}, Fe_{2p_{3/2}}, and Pb_{4f_{5/2}} and _{7/2} are depicted in Fig. 6. Nevertheless, only the clear spectra obtained from a site are included in the figure.

The As_{3d} spectra of site A and B did not show any distinct peaks, due to the low concentrations. These results are in line with the geochemical fractionation of sites A and B where the residual As was dominated at these sites. A broad peak of As(O) was observed at topsoil of site C around 44.2 eV. The dominant peaks of As(III) were observed in a soil profile of 0–40 cm at 43.4–43.9 eV (Jung et al., 2015). However, at 40–50 cm the spectra showed a weak peak of As(III). Another dominant specie of As found in this soil was of As_{4S₄} at 43.0–43.4 eV. It verifies the results of geochemical fractionation of As at site C which depicted the As bound to sulfide fractions in this area. In the 20–30 cm depth, a broad peak of As_{2O₃} was observed at 44.1 eV (Ubaid et al., 2019). The As_{3d_{5/2}}

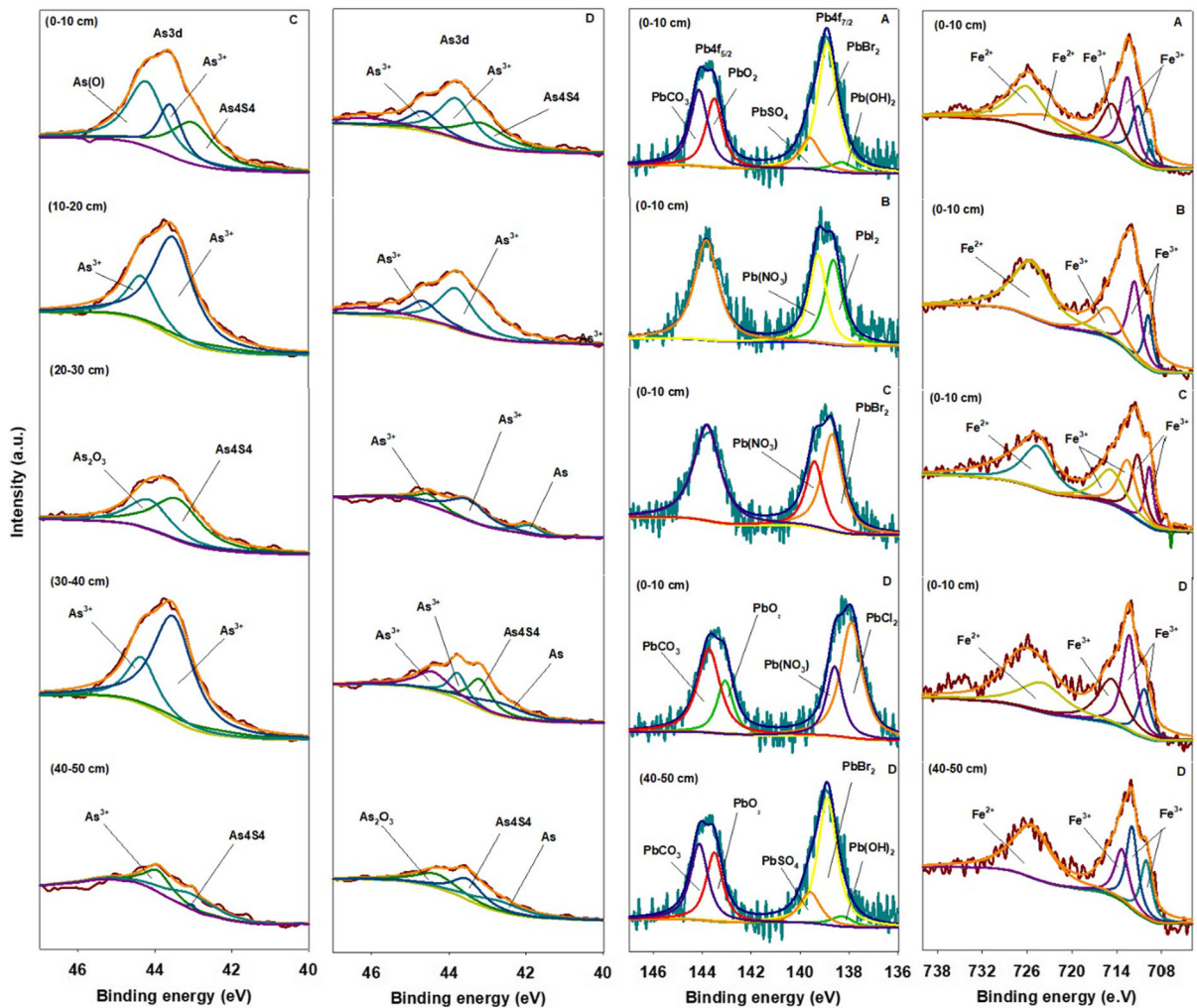


Fig. 6 The XPS spectra of As, Pb and Fe of soil samples from 0–50 cm depth of four cities **a** Abbottabad, **b** Haripur, **c** Attock, **d** Islamabad

spectra of site D depicted the same oxidation states of As at site C. However, the peaks of metallic As appeared at 41.9, 42.6, 42.6 eV at 20–30, 30–40 and 40–50 cm depth, respectively. The XPS spectra revealed that As in soils at both sites is present in the form of As (III) and no dominant peak of As (V) was observed. Under redox reactions, As(III) is oxidized supported by clay minerals and oxidation of As (III–V) is favorable for immobilization of As (III) (Wang et al., 2019). The mobility and toxicity of As(III) in the soil are much more as compared to As (V) since As (V) has a higher ability to sorb in minerals (Ferreira et al., 2019).

Pb4f_{5/2} and Pb4f_{7/2} spectra of surface soils of four sites are depicted in Fig. 6. The dominant peaks at 144.1 and 143.5 eV observed for Pb4f_{5/2} spectra were attributed to PbCO₃ and PbO₂ at site A and a peak observed at 139.5 attributed to PbSO₄, 138.8 as PbBr₂ and a small peak of Pb(OH)₂ was assigned at 138.2 eV. The Pb carbonates, sulfate, and oxides were found at the reclamation sites of automobile batteries (Cao et al., 2008). At sites B and C, no peaks were found in Pb4f_{5/2} spectra and two peaks of Pb4f_{7/2} were observed of Pb(NO₃)₂ around 139.2 and 139.4, respectively. The Pb4f_{5/2} spectra of site D also showed a broad peak of PbCO₃ at 144.0 eV and PbO₂ at 143.4 eV. The Pb4f_{7/2} spectra of site D revealed two

distinct peaks at 139.3 eV as Pb(NO)₃ and 138.7 as PbCl₂. The presence of Pb oxide, chloride and carbonate species in this site is also verified by XRD results. The broad peaks of Fe²⁺ and Fe³⁺ were found in the soil samples of all sites. The results of EF revealed anthropogenic activities involved in the enrichment of Pb and As in the study area. However, the contribution from a particular source is yet to be identified through isotopic printing.

Conclusions

This study examined the soils of the upper Indus basin for PTMs concentration, and factors affecting their behavior in the soil. The vertical distribution of targeted metal(oid)s differed among the metal(oid)s and four sites. The EF results illustrated the contribution from anthropogenic sources in the metal enrichment. Soils were found enriched with As, Cu, Ni, Pb, and Zn. Geochemical fractionation of these metals revealed that a considerable amount of these metals is present in potentially bioavailable fractions. However, generally, the percentage of residual fractions increased from top to bottom layers. The soil in the study area was found rich in organic matter and capable of retaining PTMs as FTIR analysis revealed dominant peaks in the mid-infrared region. The main mineral phases present in the soil were identified as zeolite and silicon oxides. The XPS results confirmed the presence of Pb oxides, carbonates, and chloride. These species of Pb are known to be present at sites contaminated with Pb. Furthermore, XPS results revealed dominant peaks of As (III) at site C and D for which the sources are yet to be explored. In the future, the sources of these metals in the region should be explored through isotopic imprints and remedial measures should be taken to avoid the further toxicity of soil.

Acknowledgements We acknowledge editors and reviewers for polishing the language of the paper and for in-depth discussion.

Funding The authors acknowledge the support from the National Natural Science Foundation of China (No. 41173032) and Key Program for Science and Technology Development of Anhui Province (No. 1804b06020358).

Declarations

Conflict of interest The authors declare that there is no conflict of interest.

References

- Ali, S. M., & Malik, R. N. (2010). Spatial patterns of vegetation with underlying soil properties prevailing along drain side areas in Islamabad city. *Pakistan Journal of Botany*, 42(4), 2397–2410
- Bernier, M.-H., Levy, G. J., Fine, P., & Borisover, M. (2013). Organic matter composition in soils irrigated with treated wastewater: FT-IR spectroscopic analysis of bulk soil samples. *Geoderma*, 209–210, 233–240. <https://doi.org/10.1016/j.geoderma.2013.06.017>
- Bidar, G., Waterlot, C., Verdin, A., Proix, N., Courcot, D., Détriché, S., et al. (2016). Sustainability of an in situ aided phytostabilisation on highly contaminated soils using fly ashes: Effects on the vertical distribution of physico-chemical parameters and trace elements. *Journal of Environmental Management*, 171, 204–216. <https://doi.org/10.1016/j.jenvman.2016.01.029>
- Butler, B. M., O'Rourke, S. M., & Hillier, S. (2018). Using rule-based regression models to predict and interpret soil properties from X-ray powder diffraction data. *Geoderma*, 329, 43–53. <https://doi.org/10.1016/j.geoderma.2018.04.005>
- Cao, X., Ma, L. Q., Singh, S. P., & Zhou, Q. (2008). Phosphate-induced lead immobilization from different lead minerals in soils under varying pH conditions. *Environmental Pollution*, 152(1), 184–192. <https://doi.org/10.1016/j.envpol.2007.05.008>
- Chauhan, R., Kumar, R., & Sharma, V. (2018). Soil forensics: A spectroscopic examination of trace evidence. *Microchemical Journal*, 139, 74–84. <https://doi.org/10.1016/j.microc.2018.02.020>
- De Andrade Bonetti, J., Anghinoni, I., de Moraes, M. T., & Fink, J. R. (2017). Resilience of soils with different texture, mineralogy and organic matter under long-term conservation systems. *Soil and Tillage Research*, 174, 104–112. <https://doi.org/10.1016/j.still.2017.06.008>
- Dhillon, G. S., Gillespie, A., Peak, D., & Van Rees, K. C. J. (2017). Spectroscopic investigation of soil organic matter composition for shelterbelt agroforestry systems. *Geoderma*, 298, 1–13. <https://doi.org/10.1016/j.geoderma.2017.03.016>
- El-naggar, A., Shaheen, S. M., Sik, Y., & Rinklebe, J. (2018). Biochar affects the dissolved and colloidal concentrations of Cd, Cu, Ni, and Zn and their phytoavailability and potential mobility in a mining soil under dynamic redox-conditions. *Science of the Total Environment*, 624, 1059–1071. <https://doi.org/10.1016/j.scitotenv.2017.12.190>
- Ferreira, E. P., Coelho, R. M., Valladares, G. S., da Dias, L. M. S., de Assis, A. C. C., da Silva, R. C., de Azevedo, A. C., & de Abreu, C. A. (2018). Mineralogy and concentration of

- potentially toxic elements in soils of the São Francisco sedimentary basin. *Revista Brasileira de Ciencia do Solo*, 42, 1–16. <https://doi.org/10.1590/18069657rbcs20170088>
- Farooqi, A., Masuda, H., & Firdous, N. (2007). Toxic fluoride and arsenic contaminated groundwater in the Lahore and Kasur districts, Punjab, Pakistan and possible contaminant sources. *Environmental Pollution*, 145(3), 839–849. <https://doi.org/10.1016/j.envpol.2006.05.007>
- Farooqi, A., Masuda, H., Siddiqui, R., & Naseem, M. (2009). Sources of arsenic and fluoride in highly contaminated soils causing groundwater contamination in Punjab, Pakistan. *Archives of Environmental Contamination and Toxicology*, 56(4), 693–706. <https://doi.org/10.1007/s00244-008-9239-x>
- Ferreira, N. S., Oliveira, L. H. B., Agreli, V., de Oliveira, A. F., Nogueira, A. R. A., Oliveira, A., & Gonzalez, M. H. (2019). Bioaccumulation and acute toxicity of As(III) and As(V) in Nile tilapia (*Oreochromis niloticus*). *Chemosphere*, 217, 349–354. <https://doi.org/10.1016/j.chemosphere.2018.11.013>
- Gmochowska, W., Pietranik, A., Tyszka, R., Ettler, V., Mihaljevič, M., Długosz, M., & Walenczak, K. (2019). Sources of pollution and distribution of Pb, Cd and Hg in Wrocław soils: Insight from chemical and Pb isotope composition. *Geochemistry*, 79(3), 434–445. <https://doi.org/10.1016/j.chemer.2019.07.002>
- Husnain, Eaz. (2016). *Population, labour source and employment*.
- Iqbal, J., & Shah, M. H. (2011). Distribution, correlation and risk assessment of selected metals in urban soils from Islamabad Pakistan. *Journal of Hazardous Materials*, 192(2), 887–898. <https://doi.org/10.1016/j.jhazmat.2011.05.105>
- Irshad, S., Liu, G., Yousaf, B., Ullah, H., Ali, M. U., & Rinklebe, J. (2019). Estimating the pollution characteristics and health risks of potentially toxic metal(oid)s in urban-industrial soils in the Indus basin, Pakistan. *Environmental Monitoring and Assessment*. <https://doi.org/10.1007/s10661-019-7909-y>
- Jadoon, S., Muhammad, S., Hilal, Z., Ali, M., Khan, S., & Khattak, N. U. (2020). Spatial distribution of potentially toxic elements in urban soils of Abbottabad city, (N Pakistan): Evaluation for potential risk. *Microchemical Journal*, 153, 104489. <https://doi.org/10.1016/j.microc.2019.104489>
- Jozanikohan, G., Sahabi, F., Norouzi, G. H., Memarian, H., & Moshiri, B. (2016). Quantitative analysis of the clay minerals in the Shurijeh reservoir formation using combined X-ray analytical techniques. *Russian Geology and Geophysics*, 57(7), 1048–1063. <https://doi.org/10.1016/j.rgg.2016.06.005>
- Jung, E., Lee, J., & Baek, K. (2015). Abiotic reductive extraction of arsenic from contaminated soils enhanced by complexation: Arsenic extraction by reducing agents and combination of reducing and chelating agents. *Journal of Hazardous Materials*, 283, 454–461. <https://doi.org/10.1016/j.jhazmat.2014.09.055>
- Karim, Z., Qureshi, B. A., & Mumtaz, M. (2015). Geochemical baseline determination and pollution assessment of heavy metals in urban soils of Karachi, Pakistan. *Ecological Indicators*, 48, 358–364. <https://doi.org/10.1016/j.ecolind.2014.08.032>
- Li, S., Yang, L., Chen, L., Zhao, F., & Sun, L. (2019). Spatial distribution of heavy metal concentrations in peri-urban soils in eastern China. *Environmental Science and Pollution Research*, 26(2), 1615–1627. <https://doi.org/10.1007/s11356-018-3691-6>
- Lilli, M. A., Nikolaidis, N. P., Karatzas, G. P., & Kalogerakis, N. (2019). Identifying the controlling mechanism of geogenic origin chromium release in soils. *Journal of Hazardous Materials*, 366, 169–176. <https://doi.org/10.1016/j.jhazmat.2018.11.090>
- Ma, L. Q., & Rao, G. N. (1997). Chemical fractionation of cadmium, copper, nickel, and zinc in contaminated soils. *Journal of Environmental Quality*, 26(1), 259–264
- Miles, R. J., & Changwen, W. (2014). A 1915–2011 microscale record of soil organic matter under wheat cultivation using FTIR-PAS depth-profiling. *Agronomy for Sustainable Development*, 34(4), 803–811
- Müller, G. (1979). Schwermetallen in den redimen des rheinsveränderungenseit. *Umschau Wiss Tech*, 79(24), 778–783
- Obaid-ur-Rehman. (2010). Soil fertility and salinity status of Attock district. *Journal of Agricultural Research (Pakistan)*, 48(4), 505–516
- Parab, N., Sinha, S., & Mishra, S. (2015). Coal fly ash amendment in acidic field: Effect on soil microbial activity and onion yield. *Applied Soil Ecology*, 96, 211–216. <https://doi.org/10.1016/j.apsoil.2015.08.007>
- Rahman, M. S., Clark, M. W., Yee, L. H., Comarmond, M. J., Payne, T. E., Kappen, P., & Mokhber-Shahin, L. (2017). Arsenic solid-phase speciation and reversible binding in long-term contaminated soils. *Chemosphere*, 168, 1324–1336. <https://doi.org/10.1016/j.chemosphere.2016.11.130>
- Rehman, A., Liu, G., Yousaf, B., Zia-ur-rehman, M., Ubaid, M., Saqib, M., & FarooqJaved, M. R. Z. (2020). Characterizing pollution indices and children health risk assessment of potentially toxic metal(oid)s in school dust of Lahore Pakistan. *Ecotoxicology and Environmental Safety*, 190, 110059. <https://doi.org/10.1016/j.ecoenv.2019.110059>
- Rehman, I., Ishaq, M., Ali, L., Khan, S., Ahmad, I., Din, I. U., & Ullah, H. (2018). Enrichment, spatial distribution of potential ecological and human health risk assessment via toxic metals in soil and surface water ingestion in the vicinity of sewakht mines, district Chitral, Northern Pakistan. *Ecotoxicology and Environmental Safety*, 154, 127–136. <https://doi.org/10.1016/j.ecoenv.2018.02.033>
- Ruiz-Fernández, A. C., Sanchez-Cabeza, J. A., Pérez-Bernal, L. H., & Gracia, A. (2019). Spatial and temporal distribution of heavy metal concentrations and enrichment in the southern gulf of Mexico. *Science of the Total Environment*, 651, 3174–3186. <https://doi.org/10.1016/j.scitotenv.2018.10.109>
- Shaheen, S. M., Abdelrazek, M. A. S., Elthoth, M., Moghanm, F. S., Mohamed, R., Hamza, A., El-Habashi, N., Wang, J., & Rinklebe, J. (2019). Potentially toxic elements in saltmarsh sediments and common reed (*Phragmites australis*) of burullus coastal lagoon at north Nile delta, Egypt: A survey and risk assessment. *Science of the Total Environment*, 649, 1237–1249. <https://doi.org/10.1016/j.scitotenv.2018.08.359>

- Shahid, M., Khan, N., Dumat, C., Naidu, R., Khalid, S., Mahmudur, M., & Bibi, I. (2018). A meta-analysis of the distribution, sources and health risks of arsenic-contaminated groundwater in Pakistan. *Environmental Pollution*, 242, 307–319. <https://doi.org/10.1016/j.envpol.2018.06.083>
- Singh, V., & Agrawal, H. M. (2012). Qualitative soil mineral analysis by EDXRF, XRD and AAS probes. *Radiation Physics and Chemistry*, 81(12), 1796–1803. <https://doi.org/10.1016/j.radphyschem.2012.07.002>
- Sun, J., Yu, R., Hu, G., Su, G., & Zhang, Y. (2018). Tracing of heavy metal sources and mobility in a soil depth profile via isotopic variation of Pb and Sr. *CATENA*, 171, 440–449. <https://doi.org/10.1016/j.catena.2018.07.040>
- Sun, Z., & Chen, J. (2018). Risk assessment of potentially toxic elements (PTEs) pollution at a rural industrial wasteland in an abandoned metallurgy factory in north China. *International Journal of Environmental Research and Public Health*. <https://doi.org/10.3390/ijerph15010085>
- Tariq, M., Saeed, A., Nisar, M., Mian, I. A., & Afzal, M. (2011). Effect of potassium rates and sources on the growth performance and on chloride accumulation of maize in two different textured soils of Haripur Hazara division. *Sarhad Journal of Agriculture*, 27(3), 415–422
- Thiombane, M., Di Bonito, M., Albanese, S., Zuzolo, D., Lima, A., & De Vivo, B. (2019). Geogenic versus anthropogenic behaviour and geochemical footprint of Al, Na, K and P in the Campania region (Southern Italy) soils through compositional data analysis and enrichment factor. *Geoderma*, 335, 12–26. <https://doi.org/10.1016/j.geoderma.2018.08.008>
- Ubaid, M., Liu, G., Yousaf, B., Ullah, H., & Irshad, S. (2019). Evaluation of floor-wise pollution status and deposition behavior of potentially toxic elements and nanoparticles in air conditioner dust during urbanistic development evaluation of floor-wise pollution status and deposition behavior of potentially toxic. *Journal of Hazardous Materials*, 365, 186–195. <https://doi.org/10.1016/j.jhazmat.2018.11.005>
- Van Poucke, R., Ainsworth, J., Maesele, M., Ok, Y. S., Meers, E., & Tack, F. M. G. (2018). Chemical stabilization of Cd-contaminated soil using biochar. *Applied Geochemistry*, 88, 122–130. <https://doi.org/10.1016/j.apgeochem.2017.09.001>
- Wan, X., Dong, H., Feng, L., Lin, Z., & Luo, Q. (2017). Comparison of three sequential extraction procedures for arsenic fractionation in highly polluted sites. *Chemosphere*, 178, 402–410. <https://doi.org/10.1016/j.chemosphere.2017.03.078>
- Wang, J., Liu, G., Lu, L., Zhang, J., & Liu, H. (2015). Geochemical normalization and assessment of heavy metals (Cu, Pb, Zn, and Ni) in sediments from the Huaihe river, Anhui, China. *CATENA*, 129, 30–38. <https://doi.org/10.1016/j.catena.2015.02.008>
- Wang, L., Cho, D. W., Tsang, D. C. W., Cao, X., Hou, D., Shen, Z., Alessi, D. S., Ok, Y. S., & Poon, C. S. (2019). Green remediation of As and Pb contaminated soil using cement-free clay-based stabilization/solidification. *Environment International*, 126, 336–345. <https://doi.org/10.1016/j.envint.2019.02.057>
- WanZhangZengHuangHuHuangWuWang, J. C. G. D. L. C. H. L. (2016). Synthesis and evaluation of a new class of stabilized nano-chlorapatite for Pb immobilization in sediment. *Journal of Hazardous Materials*, 320, 278–288. <https://doi.org/10.1016/j.jhazmat.2016.08.038>
- Wen, J., Li, Z., Huang, B., Luo, N., Huang, M., Yang, R., et al. (2018). The complexation of rhizosphere and nonrhizosphere soil organic matter with chromium: Using elemental analysis combined with FTIR spectroscopy. *Ecotoxicology and Environmental Safety*, 154(January), 52–58. <https://doi.org/10.1016/j.ecoenv.2018.02.014>
- Xing, Z., Du, C., Tian, K., Ma, F., Shen, Y., & Zhou, J. (2016). Application of FTIR-PAS and raman spectroscopies for the determination of organic matter in farmland soils. *Talanta*, 158, 262–269. <https://doi.org/10.1016/j.talanta.2016.05.076>
- Xing, Z., Tian, K., Du, C., Li, C., Zhou, J., & Chen, Z. (2019). Agricultural soil characterization by FTIR spectroscopy at micrometer scales: Depth profiling by photoacoustic spectroscopy. *Geoderma*, 335, 94–103. <https://doi.org/10.1016/j.geoderma.2018.08.003>
- Zhang, X., Yang, H., & Cui, Z. (2018). Evaluation and analysis of soil migration and distribution characteristics of heavy metals in iron tailings. *Journal of Cleaner Production*, 172, 475–480. <https://doi.org/10.1016/j.jclepro.2017.09.277>
- Zhou, G., Sun, B., Zeng, D., Wei, H., Liu, Z., & Zhang, B. (2014). Vertical distribution of trace elements in the sediment cores from major rivers in east China and its implication on geochemical background and anthropogenic effects. *Journal of Geochemical Exploration*, 139, 53–67. <https://doi.org/10.1016/j.gexplo.2013.03.007>

Publisher's Note Springer Nature remains neutral with regard to jurisdictional claims in published maps and institutional affiliations.